

**Fermi National Accelerator Laboratory**

**FERMILAB-Pub-96/451**

## **Simulation Studies of Ionization Cooling**

David Neuffer and A. Van Ginneken

*Fermi National Accelerator Laboratory  
P.O. Box 500, Batavia, Illinois 60510*

December 1996

Submitted to *Nuclear Instruments and Methods*

Operated by Universities Research Association Inc. under Contract No. DE-AC02-76CH03000 with the United States Department of Energy

## **Disclaimer**

*This report was prepared as an account of work sponsored by an agency of the United States Government. Neither the United States Government nor any agency thereof, nor any of their employees, makes any warranty, expressed or implied, or assumes any legal liability or responsibility for the accuracy, completeness, or usefulness of any information, apparatus, product, or process disclosed, or represents that its use would not infringe privately owned rights. Reference herein to any specific commercial product, process, or service by trade name, trademark, manufacturer, or otherwise, does not necessarily constitute or imply its endorsement, recommendation, or favoring by the United States Government or any agency thereof. The views and opinions of authors expressed herein do not necessarily state or reflect those of the United States Government or any agency thereof.*

## **Distribution**

*Approved for public release; further dissemination unlimited.*

# Simulation Studies of Ionization Cooling

David Neuffer and A. Van Ginneken  
Fermilab, PO Box 500, Batavia IL 60510

## Abstract

A  $\mu^+\mu^-$  collider relies on ionization cooling to compress the beam phase-space volume for maximal luminosity. In this paper we present simulations of ionization cooling which explore the various conditions needed for compression to collider conditions. These simulations are based on a maximally complete model of muon-atom interactions, including accurate distributions of multiple scattering and energy straggling effects. Particular cases such as cooling in low-Z absorbers, in active lenses, within solenoids, as well as the use of wedge absorbers for phase space exchange and the energy dependence of the cooling process, are explored. Constraints and guidelines for the development of complete cooling scenarios are discussed.

## INTRODUCTION

Recently considerable interest has developed in the concept of a  $\mu^+\mu^-$  Collider. [1, 2, 3, 4] This concept relies on ionization cooling to compress the beam phase-space volume to obtain high luminosity. The total reduction in 6-D phase-space that is required in recent scenarios is a factor of  $\sim 10^6$ , which is a factor of  $\sim 10$  in each phase space dimension, and this cooling must be completed within the muon lifetime. The cooling method which could accomplish this is ionization cooling, which has been previously described by Skrinsky et al.[5] and by Neuffer.[6] In ionization cooling, the beam loses transverse and longitudinal momentum while passing through a material medium, and regains only longitudinal momentum in acceleration cavities. Cooling by large factors requires many successive stages of energy loss and reacceleration (20 to 50 stages in some scenarios). In this process the beam will evolve from a large phase-space volume to more compressed forms, and the cooling sections and transport must change to match these. Also the ionization cooling process does not naturally cool the beam longitudinally. To obtain longitudinal cooling, the beam passes through wedge absorbers at regions of non-zero dispersion, which permits exchanges between longitudinal and (cooled) transverse phase-space, and this can be arranged to reduce the longitudinal phase space. Additional transverse cooling would then follow.

In this paper we discuss the cooling process and present the rms cooling equations, which include both coherent cooling and heating effects (rms multiple scattering and energy straggling), and discuss their key parameters. These equations do not describe the evolution of the full 6-D phase-space distribution, which includes large-angle scattering and non-gaussian energy-loss straggling, and various other nonlinearities. To explore a more complete picture, we have developed a simulation code called SIMUCOOL[7] which tracks individual particle trajectories through the cooling process, with maximally realistic scattering and straggling. The code is applied to characteristic cooling cases within the

cooling scenarios and compared with rms analyses. Results from these simulations are discussed to provide guidelines for optimal cooling configurations in a complete scenario. Future work will combine these sections with reaccelerations to test complete cooling sequences.

## IONIZATION COOLING CONCEPTS

The basic mechanism for ionization cooling ( $\mu$ -cooling) is displayed graphically in Figure 1. Muons pass through a material medium and lose energy (momentum) through ionization interactions, and this is followed by beam reacceleration in rf cavities. The losses are parallel to the particle motion, and therefore include transverse and longitudinal momentum losses; the transverse momentum losses reduce (normalized) transverse emittance. Reacceleration restores only longitudinal momentum. Multiple steps through the combined processes of transverse energy loss plus reacceleration could enable transverse cooling by large factors. However, the random process of multiple scattering in the material medium increases the rms beam divergence and therefore the emittance. Beam cooling requires that this scattering be less than the energy-loss cooling effect.

The differential equation for rms transverse cooling is [5, 6]:

$$\frac{d\epsilon_N}{ds} = -\frac{1}{\beta^2 E} \frac{dE}{ds} \epsilon_N + \frac{\beta\gamma}{2} \frac{\beta_{\perp}}{\beta} \frac{d\langle\theta_{rms}^2\rangle}{ds} = -\frac{1}{\beta^2 E} \frac{dE}{ds} \epsilon_N + \frac{\beta_{\perp} E_s^2}{2\beta^3 m_{\mu} c^2 L_R E} \quad (1)$$

where the first term is the frictional cooling effect and the second is the multiple scattering heating term. Here  $\epsilon_N$  is the normalized emittance,  $E$  is the beam energy,  $\beta = v/c$  and  $\gamma$  are the usual kinematic factors,  $dE/ds$  is the energy loss rate,  $\theta_{rms}$  is the rms multiple scattering angle,  $L_R$  is the material radiation length,  $\beta_{\perp}$  is the betatron function, and  $E_s$  is the characteristic scattering energy ( $\sim 13.6$  MeV). (The normalized emittance is related to the geometric emittance  $\epsilon_{\perp}$  by  $\epsilon_N = \epsilon_{\perp}(\beta\gamma)$ , and the beam size is given by  $\sigma_x = (\epsilon_{\perp}\beta_{\perp})^{1/2}$ .)

Similarly an equation for longitudinal cooling with energy loss can be written as:

$$\frac{d\sigma_E^2}{ds} = -2 \frac{\partial \frac{dE}{ds}}{\partial E} \sigma_E^2 + \frac{d\langle\Delta E_{rms}^2\rangle}{ds} \quad (2)$$

in which the first term is the cooling term and the second is the heating term caused by random fluctuations in the particle energy losses. Here we have chosen energy spread, rather than emittance (which is bunch-length times energy-spread), to measure the cooling (or heating) of the beam. From this equation we see that beam cooling can occur if the derivative  $\partial(dE/ds)/\partial E > 0$ . This energy loss can be estimated by the Bethe-Bloch equation:

$$\frac{dE}{ds} = 4\pi N_A r_e^2 m_e c^2 \frac{Z}{A} \left[ \frac{1}{\beta^2} \ln \left( \frac{2m_e c^2 \gamma^2 \beta^2}{I} \right) - 1 - \frac{\delta}{2\beta^2} \right] \quad (3)$$

where  $N_A$  is Avogadro's number,  $A$  and  $Z$  are the atomic weight and number of the absorbing material, and  $m_e$  and  $r_e$  are the mass and classical radius of the electron, ( $4\pi N_A r_e^2 m_e c^2 = 0.3071$  MeV cm<sup>2</sup>/gm). The ionization constant  $I$  is approximately  $16 Z^{0.9}$  eV, and  $\delta$  is the density effect factor which is small for low-energy  $\mu$ 's. (We have used  $\delta = 0$  in initial rms evaluations.) The derivative of  $dE/ds$  is negative (or naturally heating) for  $E_\mu < \sim 0.3$  GeV, and is only slightly positive (cooling) for higher energies.

The second term in eq. 2 is the emittance increase due to fluctuations in energy-loss in the beam-atom interactions. In the long-pathlength Gaussian-distribution limit, this is given approximately by:

$$\frac{d\langle \Delta E_{\text{rms}}^2 \rangle}{ds} = 4\pi (r_e m_e c^2)^2 n_e \gamma^2 \left(1 - \frac{\beta^2}{2}\right), \quad (4)$$

where  $n_e$  is the electron density in the material. This expression increases rapidly with higher energy (larger  $\gamma$ ), opposing the cooling process. After adding this energy straggling, we find that ionization cooling does not naturally provide adequate longitudinal cooling.

However, the cooling term can be enhanced by placing the absorbers where transverse position depends upon energy (a nonzero dispersion region) and where the absorber density or thickness also depends upon energy, such as in a wedge absorber. (see fig. 2). In that case the cooling derivative can be rewritten as:

$$\frac{\partial \frac{dE}{ds}}{\partial E} \Rightarrow \frac{\partial \frac{dE}{ds}}{\partial E} \Big|_0 + \frac{dE}{ds} \frac{\eta \rho'}{\beta c p \rho_0} \quad (5)$$

where  $\rho'/\rho_0$  indicates the change in density with respect to transverse position,  $\rho_0$  is the reference density associated with  $dE/ds$ , and  $\eta$  is the dispersion ( $\eta = dx/d(\Delta p/p)$ ). Increasing the longitudinal cooling rate in this manner decreases the transverse cooling by the same amount. The transverse cooling term is changed to:

$$\frac{d\varepsilon_N}{ds} = -\frac{1}{\beta^2 E} \frac{dE}{ds} \varepsilon_N + \frac{1}{\beta c} \frac{dE}{ds} \frac{\eta \rho'}{p \rho_0} \varepsilon_N \quad (6)$$

Fluctuations in energy loss at non-zero dispersion also cause fluctuations in the betatron amplitude ( $x_p$ ) at the absorber and this contributes to the rms betatron amplitude and therefore to the transverse emittance. This heating term is, approximately:

$$\Delta \varepsilon_N \cong \frac{\eta^2 (\Delta \sigma_p)^2}{2\beta_\perp p^2} \beta \gamma, \quad (7)$$

where  $(\Delta \sigma_p)$  is the rms random particle momentum loss.

Note that the coupled transverse cooling (and heating) changes occur in the same direction (i.e. horizontal or vertical) as the dispersion and wedge. However the sum of the cooling rates (over x, y, and z(or t)) remains constant. This sum can be represented, as with radiation damping, as a sum of cooling partition numbers, where the partition number is defined as the ratio of the cooling rate to the fractional momentum loss rate. For x and y emittance cooling the partition numbers are both naturally 1:

$$g_x = \frac{\frac{d\epsilon_x/ds}{\epsilon_x}}{\frac{dp/ds}{p}} = \frac{c}{\beta^2 E} \frac{dE}{ds} \bigg/ \frac{dp}{ds} = 1, \quad (8)$$

with a similar expression for  $g_y$ . The partition number for longitudinal cooling is given by:

$$g_L = \frac{\frac{d\epsilon_L/ds}{\epsilon_L}}{\frac{dp/ds}{p}} = \frac{\partial(dE/ds)}{\partial E} \bigg/ \frac{dp}{ds} \quad \text{or} \quad g_L = \frac{\frac{\partial(dp/dt)}{\partial p}}{\frac{dp/dt}{p}} \quad (9)$$

which is a function of muon energy. We have used canonical coordinates with  $s$  as the independent variable to set up the partition numbers, and we note that  $dp/dt = dE/ds$ .

With wedge enhancement of longitudinal cooling,  $g_x$  becomes:  $g_x = 1 - \frac{\eta\rho'}{\rho_0}$ ,

while  $g_L$  increases by  $\eta\rho'/\rho_0$ , leaving the sum of the partition numbers ( $g_x + g_y + g_L$ ) as a constant. This sum is a function of muon momentum, and the sum of the partition numbers is displayed in figure 3. The sum is approximately 2 for  $p_\mu > 0.3$  GeV/c, but is smaller for lower energies. However, as pointed out by Palmer[8], the sum does remain positive for all energies, which indicates that cooling remains possible even at low  $\mu$  energies.

Some guidelines for optimum cooling can be obtained from equations (1) - (4) and the partition functions. A useful quantity to consider is the equilibrium transverse emittance, which is obtained by solving equation 1 for  $d\epsilon_x/ds = 0$ , obtaining

$$\epsilon_{N,eq} = \frac{\beta_\perp E_s^2}{2\beta m_\mu c^2 L_R (dE/ds)}, \quad (10)$$

which should be minimized. These equations indicate that it is desirable to obtain small  $\beta_\perp$  (strong focusing) in the absorbers. It is also desirable to have materials with large values of the product  $L_R dE/ds$ , and this is maximal for light element absorbers (e. g. lithium (Li) or beryllium (Be); see Table 2.). Eq. 4 indicates that energy straggling increases greatly with high energies, while the partition function sum becomes small for low energies (figure 3). An optimum for cooling with minimal heating would occur at the intermediate values; that is,  $\gamma \cong 3$  (where  $p_\mu \cong 300$  MeV/c or  $B\rho \cong 1$  T-m), where the partition number sum is  $\sim 2$ .

## FOCUSING CONSIDERATIONS

To minimize multiple-scattering emittance growth, it is desirable to obtain small  $\beta_{\perp}$  (strong focusing) in the absorbers. Several focusing configurations have been considered, and are explored in the simulation studies. These include focusing by magnetic quadrupoles, focusing by an active current within a conducting absorber (Be or Li lens), and focusing by solenoids. Other possibilities such as plasma lenses can be considered.

### Quadrupole Focusing

It is straightforward to use a string of magnetic quadrupoles to focus the beam into a relatively small spot (small  $\beta_{\perp}$ ) at the absorber, similar to that obtained in a collider interaction region.

The equation for quad focusing in a transport region is:

$$\frac{d^2 A_x}{ds^2} \pm \frac{B'}{B\rho} A_x + \frac{1}{A_x^3} = 0 \quad (11)$$

where  $A_x = (\beta_x)^{1/2}$  is the horizontal amplitude function, and a similar equation follows for  $A_y$ , the vertical amplitude.  $B\rho = p/e$  is the particle magnetic rigidity,  $B'(s)$  is the magnetic gradient, which is opposite in sign for horizontal and vertical motion. That sign will change as the quad strengths alternate from horizontally focusing to defocusing. Quads are limited by the fact that magnetic quadrupoles focus in only one transverse direction at a time; focusing in both directions requires alternating lenses, and the beam size can increase unacceptably in the defocused plane. Also the length of a low- $\beta^*$  absorber region is limited to  $L \approx \beta^*$  (where  $\beta^*$  is the minimum value of  $\beta_{\perp}$  at the absorber) by the absence of focusing in that region, and many such absorber regions are thus required for low- $\beta_{\perp}$  cooling.

### Solenoid focusing

Some of the quad difficulties are alleviated by the use of solenoidal focusing; that is, focusing by a longitudinal field  $B_z(s)$ . The equation of amplitude motion becomes:

$$\frac{d^2 A}{ds^2} - \left( \frac{B_z}{2B\rho} \right)^2 A + \frac{1}{A^3} = 0 \quad (12)$$

Here  $A(s)$  represents both horizontal and vertical amplitudes ( $A(s) = (\beta_x)^{1/2} = (\beta_y)^{1/2}$ ), since the solenoid naturally focuses equally in both planes. Solenoidal focusing also is much stronger for smaller energies (smaller  $B\rho$ ), since  $1/B\rho$  appears squared in the focusing effect.

Solenoids can focus the beams to small  $\beta^*$  at absorbers in field-free regions, similar to the use of quads discussed above. The absorber(s) could also be placed within a solenoidal field and this would provide continuous focusing, which would permit extended absorber lengths. Note

that, at solenoidal fields of 20T and  $B\rho= 1 \text{ T}\cdot\text{m}$ , a constant value of  $\beta^* = (2B\rho/B) = 0.1 \text{ m}$  can be maintained.

However, solenoid focusing is complicated by the fact that the actual focusing effect is second-order. In entering a solenoid, particles develop a toroidal momentum ( $p_\theta$ ), which is proportional to  $r$ , from the radial magnetic field at the entrance to the solenoid and the resulting  $v_z \times B_r$  force. This toroidal momentum in turn interacts with the constant  $B_z$  field in the body of the solenoid to obtain a radial focusing force. Particles within a solenoid thus do not have simple radial focusing motion, but follow toroidal orbits with amplitudes given by the Larmor radius:  $r_L = p_\perp/eB$ [9].

This effect can be quantified by noting that the beam when entering a solenoid obtains an angular velocity given from Busch's theorem:

$$\frac{d\theta}{dz} = -\frac{qB}{2m\gamma v_z}, \quad (13)$$

which implies an angular momentum term from

$$p_\theta = xy' - yx' = \left( \langle x^2 \rangle + \langle y^2 \rangle \right) \frac{d\theta}{dz}. \quad (14)$$

This changes the projected transverse (unnormalized) emittance, which is calculated using:

$$\epsilon_x^2 = \langle x^2 \rangle \langle x'^2 \rangle - \langle xx' \rangle^2, \quad (15)$$

by adding a term equal to  $\langle y^2 \rangle (d\theta/dz)^2$  to  $\langle x'^2 \rangle$ . With cylindrical symmetry  $\langle y^2 \rangle = \langle x^2 \rangle$ , we find that the projected emittance becomes:

$$\epsilon_x^2 = \epsilon_{x0}^2 + \langle x^2 \rangle^2 \left( \frac{d\theta}{dz} \right)^2. \quad (16)$$

where  $\epsilon_{x0}$  is the emittance prior to entering the solenoid. In exiting the solenoid the process is reversed, with  $p_\theta$  subtracted from the particle momentum, and the projected emittance is restored to its pre-solenoid value. With an absorber within the solenoid, the beam loses angular momentum within the absorber, and when the beam exits the solenoid it retains a net angular momentum. If it is uncompensated, this angular momentum results in emittance dilution.

Even without an absorber within the solenoid, matching from inside to outside of solenoidal fields is in general complicated by the toroidal orbits, and by the transition fields within which these orbits develop. Particles with insufficient momenta will be reflected by these fields, and other particles will have their 6-D motion unacceptably distorted.

In the simulations discussed below we consider cases in which the absorber is either at a field-free focus produced by solenoids, or the absorber is within a solenoidally focusing region.

Particle tracking includes complete dynamics within solenoids and within transition magnetic fields.

### Active Lens Absorber (conductor such as Li or Be)

The optical constraint on useable absorber length ( $L < \beta^*$ ) can also be removed if the absorber is an active focusing lens. The absorber is an active lens when it is a conducting cylinder containing a large pulsed current, as occurs in a Li lens. A uniform current density within a cylinder of radius  $R$  produces an azimuthal magnetic field given by:

$$B_{\theta} = \frac{\mu I r}{2\pi R^2} \quad (17)$$

where  $\mu \equiv \mu_0 = 4\pi \times 10^{-7}$  (MKS), and  $I$  is the total current.[10] This produces a linear radial focusing force, which provides focusing for both transverse amplitude functions, in the equation:

$$\frac{d^2 A_x}{ds^2} - \frac{B'}{B\rho} A_x + \frac{1}{A_x^3} = 0 \quad (18)$$

where  $B' = dB/dr$ . With  $B' = 1600$  T/m,  $B\rho = 1$  T-m ( $p=0.3$  GeV/c), an equilibrium betatron function of  $\beta^* = (B\rho/B')^{1/2} = 0.025$  m would be obtained, and cooling over an extended absorber at this  $\beta^*$  could be developed. This gradient could be further increased and  $B\rho$  decreased to obtain even smaller  $\beta^*$ , perhaps to  $\sim 0.01$  m, but probably not much smaller.

### Wedges and Phase Space Exchange

Since ionization cooling naturally provides very little longitudinal cooling, the 6-D cooling process requires periodic exchanges of phase space between transverse and longitudinal degrees of freedom. As shown in figure 2, these can be obtained by passing the beam through wedges in regions where there is a non-zero dispersion (position-dependence on momentum), that is:

$$x = x_{\beta} + \eta\delta. \quad (19)$$

where  $\delta = \Delta p/p$ ,  $\eta$  is the dispersion and  $x_{\beta}$  indicates the momentum-independent transverse betatron motion of the particles. The wedge is characterized by its effect on the momentum offset  $\delta$  of particles:

$$\delta \rightarrow \delta - \frac{(dp/ds) \tan \theta}{p} x = \delta - \delta'(\eta\delta + x_{\beta}) \quad (20)$$

$dp/ds$  is the momentum loss rate in the material ( $dp/ds = \beta^{-1}dE/ds$ ), which depends upon the material and the particle energy. The wedge thickness at a transverse position  $x$  (relative to the

central orbit at  $x=0$ ) is  $x \tan\theta$ , and the symbol  $\delta' = (dp/ds)\tan\theta / p$  indicates the change of  $\delta$  with  $x$ .

The emittance exchange process is described in greater detail in reference [11]. Following ref. [11], in a first approximation we can ignore the cooling from the average energy loss and separate out the position-dependent portion of the energy loss, which gives an emittance exchange. With the wedge oriented so that higher-energy beam passes through more material, the energy spread is reduced. The momentum width is changed from  $\delta_0$  to:

$$\delta_1 = \delta_0 \left[ (1 - \eta_0 \delta')^2 + \frac{\delta'^2 \sigma^2}{\delta_0^2} \right]^{1/2}. \quad (21)$$

The bunch length is unchanged. The longitudinal emittance, the area of the beam in longitudinal phase-space (energy-width  $\times$  bunch-length), is changed simply by the ratio of energy-widths, which means that the longitudinal emittance changes by the factor  $\delta_1/\delta_0$ .

From emittance conservation, the transverse emittance (in the dispersion plane) is changed by the inverse of the momentum width decrease factor:

$$\varepsilon_1 = \varepsilon_0 \left[ (1 - \eta_0 \delta')^2 + \frac{\delta'^2 \sigma^2}{\delta_0^2} \right]^{-1/2}. \quad (22)$$

As described in ref. [11], the betatron functions ( $\eta$ ,  $\beta$ ) are also changed by the absorber. It is possible to arrange  $\eta$  and the wedge thickness so that the dispersion is cancelled to zero, which can simplify the optics. This occurs if

$$\delta' = \frac{1}{\eta_0 \left[ 1 + \frac{\sigma_0^2}{\eta_0^2 \delta_0^2} \right]}. \quad (23)$$

If the wedge is oriented so that higher energy beam passes through less absorber (that is,  $\delta' < 0$ ), then energy spread and longitudinal emittance increases while transverse emittance decreases from emittance conservation. This “inverse” exchange can be used to minimize final transverse emittance in some cooling scenarios. [8]

All transverse changes occur in the plane of the dispersion (horizontal for horizontal bends), while the other transverse plane is unchanged. The effects can be balanced by alternating horizontal and vertical bend/wedge sections.

The wedge also has cooling from the average energy loss, as well as emittance dilution from energy straggling, multiple scattering, and the emittance dilution from energy straggling at non-zero dispersion. These effects must be included in a complete model, and are included in the simulations.

## SIMULATION METHODS AND APPROXIMATIONS

Simulation of particle transport through a cooling section starts from a description of the phase space of the incident muons. To evaluate the cooling progress the kinematic variables of the particles are noted upon crossing some fixed set of planes perpendicular to the central trajectory—including the start and finish of the absorber. For a Hamiltonian formulation, this makes  $z$ , the distance along the nominal trajectory, the logical choice of independent variable, with time and energy as canonical dependent variables. Thus normalized phase space is then best described by the transverse variables  $x$ ,  $p_x$ ,  $y$ ,  $p_y$ , and longitudinally by  $t$  and  $E$ , and we will use these variables in analysis of the simulation results.

The cooling channel may include absorbers of arbitrary composition and dimensions as well as magnetic fields of arbitrary specification. Absorber material and magnetic field as a function of location are supplied to desired accuracy either by a field map or by an analytical prescription. Except when traversing a field-free void or a void in which the field is simple enough to permit an exact analytic description of the trajectories, particles are traced through the absorber geometry in a series of small steps—each typically of the order of a few mm.

The step length is chosen according to two criteria: the interaction of the muon with the absorber material, and the strength and variation of the magnetic-field forces. The material step length is chosen as a compromise between speed and accuracy, but remains the same within a given material. These choices allow adequate sampling of the field and absorber material along particle paths and result in a close approximation to actual trajectories.

### Interactions in Absorbers

The physics content of SIMUCOOL is essentially unchanged from that presented in some detail in ref. [7]. Briefly, the main ingredients are: *ionization energy loss* as described by the Vavilov distribution modified for spin one-half particles and with inclusion of an energy threshold above which  $\mu$ -e collisions are simulated individually, and *multiple Coulomb scattering*, in which an angular threshold is adopted below which it is treated in the Gaussian approximation and above which as coherent individual  $\mu$ -nucleus scattering events. Lesser contributions—especially at the lower energies of interest here—are incoherent Coulomb scattering between muons and nuclear protons, bremsstrahlung,  $e^+e^-$  production, and deep inelastic  $\mu$ -nucleus collisions. The (modified) Vavilov distribution is in the form of an integral which—as noted in ref. [7]—is not well suited to direct Monte Carlo sampling. Instead, for each absorber material of interest a set of tables of the distribution is prepared. Each table corresponds to a definite muon momentum and the entries in the table correspond to the (cumulative) probability of undergoing a predetermined energy loss. Typical table-to-table momentum spacing is  $\sim 0.02\text{GeV}/c$ . The tables assume a fixed absorber thickness, i.e., a fixed step-length in the simulation. When

choosing a (random) energy loss—a la Vavilov—during the calculation one selects first the appropriate table on a random basis (with a linear interpolation) between the two tables adjacent to the muon's momentum, after which one chooses the energy loss directly from that table with linear interpolation between table entries. The energy loss so determined is relative to the mean (restricted) energy loss over the trajectory. The latter is calculated as per eq. (22.5) of ref. [12] with the density effect parametrization as in ref. [13]. For elemental targets the necessary parameters to calculate  $\delta$  are provided by the program while for compounds they must be supplied specifically. For an incomplete step, as when crossing a plane where analysis is performed, the energy loss is estimated as being proportional to that for a full step.

Energy loss and multiple scattering are treated as continuous processes and are thus applied during each step of the Monte Carlo which takes place in material. All other processes, including large energy losses and large angle scattering, are treated event-by-event. Any number of such events may occur in a single step including zero events—usually the most probable outcome. To minimize bias the order in which results of the various processes are calculated is randomly shuffled at each step. If one or more events of a given type occur, the result is a change in the muon's direction or energy or both. Included in the shuffle is the change in position during the step as well as the magnetic deflection when a field is present.

### **Magnetic Tracking**

It is convenient to have an algorithm which can quickly and accurately calculate changes in position and momentum components in an arbitrary—user supplied—field. For a simple field in a void, speedier execution may result if one supplies the necessary code to traverse the region in one or more large steps. However one should examine the validity of any approximations involved in such large scale transport. This pertains, e.g., to the linear optics used in high energy accelerator studies which may become invalidated by the low momenta and large angles encountered in the typical  $\mu$ -cooling scenario. One can ascertain this by comparisons with the general algorithm presented here which can be set to essentially arbitrary accuracy.

In this (iterative) algorithm, position and momentum components are evaluated in accord with the particle's helical trajectory about the local field direction evaluated at (projected) mid-step. The length of the first step is the material step length. Next, the step size is halved and coordinates and direction are determined after two steps, and compared with the single step results. This algorithm continues until some minimal convergence is achieved, viz., that successive iterates of all coordinates and direction cosines differ by less than some small parameter which is set by the user. (For all cases presented here it is  $10^{-6}$  cm for the coordinates and  $10^{-6}$  for the direction cosines.)

At each stage the 'best' estimates are obtained by (Richardson) extrapolation to zero step size of the last three results. In particular, the interpolative polynomial is assumed to be quadratic in  $s^2$ :  $a + b s^2 + c s^4$ . It is even in  $s$  because convergence should be achievable

equally well from either side at any point of the trajectory. It also has zero slope at  $s = 0$ , which—absent singularities—is to be expected when  $s$  becomes so small that no significant variation of the field occurs over this distance. The best estimate for  $x$  (or other coordinate) thus corresponds to  $a$  in the above expression which, when solved as a linear system for the last three calculated  $x$ -values ( $x_j, x_{j-1}, x_{j-2}$ ), becomes  $x = (64 x_j - 20 x_{j-1} + x_{j-2})/45$  at any stage of the algorithm. Little is to be gained from higher order polynomials: adding an additional term with a cubic in  $s^2$  gives an  $x_{j-3}$  coefficient which is only  $1/2835$  while the coefficients of the other three do not change much. Any improvement in the estimation is offset by the extra computation. At a minimum the algorithm goes through two steps—at which point the extrapolation is performed with  $c = 0$ , in which case  $x = (4 x_j - x_{j-1})/3$ , etc. For a relatively weak field this may already suffice to reach convergence.

## Output

At the end of the cooling section and at a few points along the way, i.e., at some values of  $z$  to be specified, the progress of cooling is analyzed. In addition to various phase space plots a covariance matrix of the six dimensional phase space is obtained. The (square root of the) determinant of this matrix is a measure of the phase space and therefore of any cooling achieved. This is adequate whenever the phase space resembles a 6-D Gaussian ellipsoid. It remains a useful measure as long as any more complicated structures, such as nonlinear correlations, appearing in the phase space are irreversible—at least for practical purposes. But when such structure is expected to be removed at a later stage (by a nonlinear transport or absorber) the determinant overestimates the phase space volume, and one must evaluate it by other means.

In addition to 6-D phase space volume, 2-D volumes as measured by the  $\{x, p_x\}$ ,  $\{y, p_y\}$  and  $\{E, t\}$  sub-determinants are obtained. Where one expects strong mixing among just two of the 2-D spaces it is useful to keep track of some particular 4-D spaces, in order to accurately gauge phase-space dilution. For the cases treated here, solenoids strongly mix  $\{x, p_x\}$  and  $\{y, p_y\}$ , while for an x-wedge  $\{x, p_x\}$  and  $\{E, t\}$  are mixed.

## PARTICULAR CASES AND EXPLORATIONS

While a full cooling scenario has not yet been completely specified, its general properties can be inferred from the physics constraints in ionization cooling. In a complete scenario the beam is cooled from an initial transverse emittance of  $\sim 0.015$  m-rad (normalized) to  $\sim 0.00005$  m-rad. In longitudinal space, the energy spread is reduced from  $\sim 10\%$  to  $\sim 1\%$ , and the bunch length varies from an initial value of 1m to  $\sim$ cm or less within the cooling process, although finishing at  $\sim$ 1m lengths. The central beam momentum varies from  $\sim 500$  MeV/c to 100 MeV/c, and cooling is obtained by multiple steps of energy loss in absorbers followed by reacceleration. In each absorber step, the energy loss and the resulting cooling is  $< \sim 50\%$ . In this section we report results of cooling simulations in various absorbers under a variety of focusing conditions and energies, all corresponding to possible steps in a complete scenario.

## Field-free Absorber

The simplest cooling case is that of a field-free absorber placed at a focus of the beam. In table 1 we present simulation results for a sample of cooling situations, along with some comparisons with rms formula results. In each of these cases the beam is focused to a waist with a focusing parameter  $\beta_1^*$  of half the absorber length at the absorber center (which means that  $\beta_1^* = \text{absorber length}$ , and  $\alpha^*=1$  at the entrance of absorber). A distribution of 5000—25000 particles is generated randomly within gaussian distributions in  $x, p_x, y, p_y, t, E$  space and tracked through the absorber. A reference initial bunch length of 1 ns is used without reoptimization. Final beam parameters are compiled and rms quantities ( $\langle x^2 \rangle, \langle x x' \rangle$ , etc.) calculated. Transverse rms emittances are obtained from ( $\langle x^2 \rangle, \langle x x' \rangle, \langle x'^2 \rangle$ ), with a similar evaluation for  $y$ , and 6-D emittances are obtained from the full 6-D phase space determinant. The rms evaluations shown below do not directly include the deviations from gaussian distributions in the ionization or nonlinear correlations. The evaluations are therefore pessimistic; some of these correlations and nonlinearities can be removed in beam matching. In general we want an absorber with high density (to maximize energy loss within a given focus length) and low-Z (to minimize multiple scattering). Be ( $Z=4, \rho=1.85 \text{ gm/cc}$ ) is chosen as a representative material, although other materials ( $\text{H}_2$ -low Z but low  $\rho$ , Li, LiH, C (higher Z but higher  $\rho$ ), Al, etc.) can also be used in various portions of a cooling system.

Properties of materials relevant to ionization cooling ( $dE/ds, \rho, L_R$ ) for many elements are tabulated in the Particle Data Group Review of Particle Properties [12], and we have abstracted some of these into Table 2. Ionization cooling is best for maximum  $L_R \times dE/ds$ , but higher density is also desired. (Energy loss and scattering relationships, along with references to the original literature, are also summarized in ref. 12.)

The first two cooling cases in Table 1 study cooling at 400 and  $\sim 200 \text{ MeV/c}$ , which covers the range of optimum cooling energies. The third case uses the lower density, lower-Z LiH material. In the fourth case, a very large emittance beam is cooled (similar to that expected closely following the  $\mu$  production target). Good agreement with rms estimates of transverse cooling and energy straggling is obtained, and significant 6-D emittance cooling is also obtained in each case.

Figure 4 shows transverse phase space ( $x-p_x$ ) at the entrance and the exit of the absorber for the second case. The tilts in the distributions indicate the beam is focusing or converging going into the absorber, and defocusing (diverging) at the exit. The distribution densities do increase, indicating that cooling occurs.

**Table 1: Muon cooling results-Absorbers at beam focus**

Cooling example	Be Absorber (medium energy)	Be absorber (low-energy beam)	Li H absorber	Be Absorber (large emittance)	
Absorber type, length	Be, 40 cm	Be, 20cm	LiH, 14 cm	Be, 21.5cm	
Focusing (absorber center)	20	10	7	10.75	
<b>Initial beam parameters</b>					
Kinetic Energy (E)	308	130	174	162	MeV
Momentum(p)	400	210	259	246	MeV/c
Transverse emittance	1.00	0.410	0.499	1.98	cm-radians (normalized)
Momentum spread ( $\delta p$ )	8.0	5.94	11.8	12.0	MeV/c
<b>Final beam parameters</b>					
Kinetic Energy (E)	192	61	151	87	MeV
Momentum(p)	277	129	234	160	MeV/c
Trans. emittance-simulation	0.77	0.296	0.459	1.33	cm-radians (normalized)
Trans. emittance-rms eqns.	0.75	0.295	0.456	1.38	cm-radians (normalized)
Momentum spread ( $\delta p/p$ )	10.4	9.77	12.5	13.6	
6-D emittance cooling	0.738	0.736	0.859	0.654	( $E_{N, final}/E_{N, initial}$ )

**Table 2: Material Properties for Ionization Cooling**

Material	Symbol	Z	A	dE/ds (min.) (MeV/cm)	$L_R$ (cm)	$L_R$ dE/ds	Density (gm/cm <sup>3</sup> )
Hydrogen	H <sub>2</sub>	1	1.01	0.292	865	252.6	0.071
Lithium	Li	3	6.94	0.848	155	130.8	0.534
Beryllium	Be	4	9.01	2.98	35.3	105.2	1.848
Carbon	C	6	12.01	4.032	18.8	75.8	2.265
Aluminum	Al	13	26.98	4.37	8.9	38.9	2.70
Copper	Cu	29	63.55	12.90	1.43	18.45	8.96

### Cooling Energy Dependence

Following the above explorations, we consider the variation of cooling with beam energy. The critical process here is energy straggling, which increases rapidly with energy ( $\sigma_E^2 \propto E^2$ ), and we increase the energy from 235 to 415 to 806 to 1206 MeV to find a threshold for unacceptably large straggling. Table 3 shows some simulation results of the corresponding energy sweep with fixed absorber length, and with a small initial energy spread. For 800 MeV the straggling has increased following the approximate formula ( $\delta p = \sim 8$  MeV), while for 1200 MeV it becomes very large, with an increase in  $\delta p/p$  of 1% in an absorber in which only 6% of the energy is lost. Thus ionization cooling develops unacceptably large energy straggling for  $E_\mu > \sim 1$  GeV, but energy straggling appears acceptably small for beams with lower energies, with a broad minimum at  $E \sim 400$  MeV.

Figure 5 shows energy spread before and after passing through an absorber for the 400 MeV/c case, starting from a small initial energy spread of  $\sim 2$  MeV. The increase in energy spread due to energy-straggling is visible, with a "Landau-tail" - a skewed non-gaussian distribution with an extended low-energy tail for particles with large energy losses.

Table 3: Muon cooling results-Energy Dependence of Cooling

Cooling example	211 MeV/c	400 MeV/c	800 MeV/c	1200MeV/c	
Absorber type, length	Be, 20 cm	Be, 20cm	Be, 20 cm	Be, 20cm	
Focusing (absorber center)	10	10	10	10	cm
<b>Initial beam parameters</b>					
Kinetic Energy ( $T = E - mc^2$ )	130	308	701	1099	MeV
Momentum(p)	211	400	800	1200	MeV/c
Transverse emittance	0.403	0.402	0.400	0.400	cm-radians (normalized)
Momentum spread ( $\delta p$ )	1.96	1.99	1.99	2.99	MeV/c
<b>Final beam parameters</b>					
Kinetic Energy ( $T = E - mc^2$ )	60	249	643	1036	MeV
Momentum(p)	128	339	742	1137	MeV/c
Trans. emittance-simulation	0.282	0.357	0.378	0.383	cm-radians (normalized)
Trans. emittance-rms eqns.	0.289	0.354	0.375	0.382	cm-radians (normalized)
Momentum spread ( $\delta p$ )	5.15	4.30	8.23	13.0	MeV/c (simulation)
$\delta p$ - energy straggling (eq. 5)	3.96	4.90	8.70	13.0	MeV/c (formula)

### Active lens absorbers

A current within a conductor provides an active lens absorber, which can maintain the beam at small  $\beta^*$  throughout an extended absorber length ( $L \gg \beta^*$ ). Active lens absorbers are desirable since a relatively small number of these can reduce 6-D beam emittances by large factors. Table 4 displays results for a series of four Be lens cases, with initial emittances covering the desired cooling range. Note that as the beam is cooled, smaller aperture and therefore stronger gradient and smaller  $\beta^*$  can be obtained, and this is reflected in the examples. Also the studies show that the cooling is insensitive to the initial values of  $\beta^*$  and  $\alpha$ , so that only approximate optical matching is required. We have used Be rather than Li in these cases because of the greater density and larger  $dE/ds$  of Be, although Li lens technology is more developed. Li lenses would obtain similar results with less rms scattering, but must be  $\sim 3\times$  longer to obtain the same cooling, because of the smaller  $dE/ds$ .

Figure 6 shows the  $x$ - $p_x$  phase space distribution at the beginning and at the end of the absorber in the first of these cases, and this visually displays the invariant transverse phase space cooling by a factor of  $\sim 1.67$ . Each of these four cases shows similar compression, and these cases demonstrate that a sequence of similar cooling lenses can take the beam from large to small emittances. From these cases a cooling path for  $\epsilon_N$  from  $\sim 0.02$  to  $\sim 0.0001$  m-rad can be developed.

In cooling to small emittances ( $\epsilon_N < 0.001$  m-rad), a few particles are scattered to very large amplitudes, relative to the cooled beam. If included, these few particles severely distort the rms beam parameters. However only a few particles are scattered into this category ( $< 0.1\%$ ) and can be removed by an acceptance aperture. In the present examples

a  $10\sigma$  aperture cut was used and only a few particles are rejected. (A smaller cut would have further reduced rms accepted emittances but would still have acceptable survival.)

Table 4: Muon cooling results-Active Lens absorbers

Cooling example	Be Lens large emittance	Be Lens	Be Lens	Be Lens small emittance	
Absorber type, length	Be, 60cm	Be, 60cm	Be, 60cm	Be, 60cm	
$\beta^*$ (absorber entrance)	20.2	8.2	3.65	1.16	cm
Focusing Strength	33	200	1000	10000	T/m
		Initial beam parameters			
Momentum(p)	400	400	400	400	MeV/c
Transverse emittance	1.00	0.300	0.100	0.0301	cm-radians (normalized)
Momentum spread ( $\delta p$ )	17.0	17.0	8.7	8.0	MeV/c
		Final beam parameters			
Momentum(p)	210.6	210.1	210	210	MeV/c
Trans. emittance-simulation	0.59	0.185	0.067	0.0188	cm-radians (normalized)
Trans. emittance-rms eqns.	0.596	0.189	0.066	0.020	cm-radians (normalized)
Momentum spread ( $\delta p$ )	22.6	21.9	12.6	11.9	MeV/c
6-D emittance cooling	0.416	0.455	0.59	0.54	( $E_N, final/E_N, initial$ )

### Wedge Absorbers and Transverse-Longitudinal Phase Space Exchange

Collider ionization cooling scenarios require some exchange in emittance between transverse and longitudinal degrees of freedom. These exchanges must occur throughout the cooling sequence, as transverse emittances are reduced. As discussed above, exchange can be obtained by passing the beam through wedge absorbers at non-zero dispersion regions. In Table 5, we present results of simulation of several cases, representative of characteristic emittance exchange steps.

The first example of table 5 corresponds to beam conditions near the beginning of cooling, where energy spreads and emittances are both very large. We choose a  $\mu$ -beam at an initial kinetic energy of 300 MeV, an initial rms momentum spread  $\delta_1$  of 7.4%, and rms normalized emittance of 0.015m-rad (geometric emittance of  $\epsilon_1 = 0.004$ ). The beam is focussed onto a beryllium wedge absorber ( $dE/ds = 3$  MeV/cm) with  $\beta_1 = 0.34$ m ( $\sigma = 3.7$ cm) at a dispersion of 1m; the ratio of momentum to emittance beam size is two. The example is matched to obtain small dispersion after the wedge. The wedge is designed to reduce the energy spread by  $\sim\sqrt{5}$  while increasing transverse emittance by the same factor. Even though this is a case with very large energy spread and large emittance, simulation results agree well with linear models. Without reoptimization, the dispersion is reduced from 1 m to  $\sim 0.1$  m (compared to a linear model prediction of 0.13m) and an exchange of a factor of  $\sim 2$  is obtained (rather than  $\sqrt{5} = 2.236$ ). Figure 7 shows x-E phase space before and after the wedge plus a further 17 cm of energy loss. The reduction in energy spread and dispersion (x-E slope) are displayed.

The wedge is thick enough to accommodate the full momentum spread as well as the full beam size, and is therefore thick enough that the cooling term and the scattering (rms heating terms) are both nonnegligible. With a wedge with a 17 cm thickness at the beam center the mean energy decreases  $\sim 50$  MeV in energy to 340 MeV/c. The energy-straggling and multiple-scattering heating terms explain the deviations from linear models. Also, the large energy loss results in  $\sim 10\%$  transverse (and 6-D) cooling.

The second case corresponds to conditions near the middle of the cooling sequence. The beam momentum is 200 MeV/c and a 0.035m Be wedge at  $\eta = 0.5\text{m}$  and  $\beta = 0.15\text{m}$  reduces the momentum spread from 4% to 2.5% while transverse (x) emittance is increased by a factor of 1.6. The SIMUCOOL results are in good agreement with the rms model.

**Table 5: Examples of Phase Space Exchange**

Exchange Parameter	Example 1	Example 2	Example 3
$T_{\text{beam}} (T = E - mc^2)$	300	120	25
$P_{\text{beam}}$	392	199.4	76.9
$\delta_0 = \delta p$ (initial) (MeV/c)	28.4	10.22	0.76
$\eta_0$ - initial dispersion	1.0m	0.5	-0.105
$\sigma_0$ - initial beam size	0.037m	0.017	0.001
$\beta_0$ - initial betatron function	0.34m	0.15	0.013
$\epsilon_{0,N}$ - initial transverse emittance (normalized)	0.015 m-rad	0.00402	$61 \times 10^6$
Wedge material	Be	Be	LiH
$dp/ds$ (MeV/cm)	3.0	3.4	15.8
$\tan \theta$	1.0	0.65	0.6
$\delta' = dp/ds \tan \theta/p$	0.80	1.107	0.044
Exchange factor(design)	0.44	0.625	1.60
thickness ( $2\sigma$ )	0.17	0.035	0.0017
<b>Simulation Results</b>			
$P_{\text{beam}}$	392	199.4	73.9
$\delta_f - \delta p$ final (MeV/c)	13.9	6.6	2.12
$\eta_f$ - final dispersion	0.09m	0.25	-0.047
$\epsilon_f$ - final x - emittance (normalized)	0.0276 m-rad	0.0067	$35 \times 10^6$
$\epsilon_{f,y}$ - final y emittance (normalized)	0.0135	0.00386	$67 \times 10^6$

The third case is from near the end of a cooling sequence, where the longitudinal phase space is increased in order to reduce transverse emittance (see Fig. 8), in order to obtain minimal final transverse emittances for the  $\mu^+ - \mu^-$  collider. This wedge is arranged so as to increase the energy spread, and that condition is obtained by choosing  $\tan \theta < 0$ , or, alternatively, a negative dispersion. The beam energy is 25 MeV with a normalized emittance of 61 mm-mrad and initial  $\delta = 0.0081$ , and the beam is focussed to small  $\beta^*$  (0.014m) at small dispersion (0.0105m) with a 0.0017 m thick wedge. We expect a decrease of emittance by a factor of 1.6 with a corresponding increase of  $\delta p/p$ ; SIMUCOOL results are in reasonable agreement with the simplified models.

## Cooling in Solenoids

Solenoids can provide strong focusing for lower energy  $\mu$  beams, and that focusing can be used to focus the beam into an absorber. The absorber can also be placed inside a solenoid, which can then form continuous focusing for an extended absorber. However, phase space dilution can occur because of the remanent angular momentum which the beam receives when it exits the solenoid.

In table 6 we display results of a case which shows significant cooling by an extended absorber within a focusing solenoid. In this case we transport 211 MeV/c beam within a 60 cm long Li absorber within a 7T solenoid, which maintained  $\beta^* \sim 0.2$  m. We obtain cooling of emittance to  $\sim 0.33$  cm-rad (projected, normalized), even though this contains a significant angular momentum component. Removing the angular momentum (the  $x$ - $y'$  correlation) obtains an emittance of 0.307, which indicates the emittance dilution obtained from residual angular momentum in exiting the absorber-solenoid. Here the angular-momentum effect is significant but not greater than the cooling.

Figure 9 shows a few particle trajectories within this sample case ( $x(z)$ ), illustrating projected Larmor orbits within the solenoid. We include 20 cm long transition regions where the longitudinal field rises sinusoidally from 0 to 7 T and the beam develops angular momentum. The beam is somewhat mismatched with a focus at the beginning and the end of the solenoid.

**Table 6: Example of Solenoidal Cooling**

	Example 1
$T_{\text{beam}}$ ( $T = E - mc^2$ )	130
$P_{\text{beam}}$	211
$\delta_0 = \delta p$ (initial) (MeV/c)	5.24
B-field	7T
$d\theta/ds$ ( $m^{-1}$ )	-5.05
$\sigma_0$ - initial beam size	0.0184m
$\beta_0$ - initial betatron function	0.13m
$\epsilon_{0N}$ - initial transverse emittance (normalized)	0.00403 m-rad
Absorber material	Li
$dp/ds$ (MeV/cm)	1.17
absorber Length (m)	0.60
	<b>Simulation Results</b>
Initial projected emittance (unnormalized)	0.00261 m-rad
Initial $xy'$ (ang. Momentum/2)	-0.00167m-rad
$P_{\text{beam}}$ final	141
$\delta_f = \delta p$ final (MeV/c)	8.01
$\epsilon_f$ - final emittance (projected, unnorm.)	0.00247 m-rad
$\epsilon_f$ - final emittance (projected, norm.)	0.00330 m-rad
$xy'$ final (angular momentum/2)	0.000893
$\epsilon_f$ - final emittance (angular momentum removed, norm.)	0.00307 m-rad

## Multi-step Cooling- an Initial Example

As an initial example of multistep cooling we consider cooling by a sequence of three Be lenses, each 63 cm long. Simulation results are shown in Table 7, as well as in figures 10 and 11. The beam is injected into the first lens at 400 MeV/c with a large emittance and moderately large momentum spread (the same as table 3 parameters), and with the beam size matched to the lens focusing strength. In each absorbing lens the beam loses ~200 MeV/c in total momentum. At the end of the first lens the beam is reaccelerated and a transport matrix approximately matches the beam into the entrance of the next lens. The beam is then cooled through the second lens, at the end of which it is reaccelerated and rematched into the third lens. Over the three lenses the transverse emittances are reduced by a factor of ~5 from  $\epsilon_N = 0.01$  m-rad to  $\epsilon_N = 0.002$  m-rad, while the 6-D emittance is reduced by a factor of 15. Figure 10 shows transverse phase space at the start and at the end of each lens, showing the transverse cooling. In this example, there is no wedge cooling, and the same acceleration is applied to all particles at the end of each lens. The energy spread increases from straggling, and figure 11 shows the energy distribution at the beginning and at the end of each reacceleration. The rms energy spread increases by almost a factor of two and a "Landau tail" in energy loss develops. However transverse emittance cooling continues with the enlarged momentum spread, and only a few particles are scattered to very large energy loss.

This case shows a first unoptimized multistep cooling example, and demonstrates that cooling by relatively large factors is possible with little beam loss. To develop this into a collider cooling scenario, we must add many more steps, and add wedges at non-zero dispersion periodically to reduce the energy spread. More complete models of the acceleration and beam transport must be incorporated and the entire process must be optimized.

**Table 7 - Multistep Be-lens Cooling Simulation Results**

Cooling Parameters					
Initial momentum		400 MeV/c			
Lens/absorber type		Be			
Lens/absorber Lengths		63 cm			
Parameter	Initial Value	after Lens 1	Lens 2	Lens 3	
transverse rms emittance - $\epsilon_N$	0.010	0.00568	0.00337	0.00207	m-rad
rms beam size - $\sigma_x$	2.35	2.135	1.403	0.912	cm
lens focusing strength	-	33	60	120	T/m
Transverse focusing $\beta_x$	21	14.8	10.8	6.5	cm
rms momentum spread - $\sigma_p$	17.2	22.8	27.1	31.4	MeV/c
6-D emittance	14.1	5.45	2.26	0.987	cm <sup>3</sup>
6-D emittance cooling factor	1.0	0.385	0.160	0.070	

## Discussion - Toward Complete Scenario Development

A high-luminosity  $\mu^+\mu^-$  collider requires cooling in transverse phase space from an rms transverse emittance of ~0.015 m-rad (normalized) at the  $\mu$  production source to

$\sim 0.00005$  m-rad at the end of cooling where the beam is then accelerated for collisions. Some longitudinal cooling is also required, and this corresponds to an rms energy spread decrease from  $\sim 50$  MeV to  $\sim 5$  MeV (at 3 ns bunch lengths). Multiplying these cooling requirements over horizontal, vertical and longitudinal coordinates obtains a total 6-D phase space reduction of  $\sim 10^6$ .

In this paper, results of ionization cooling simulations in a variety of absorber configurations are discussed, and these cases largely cover the range of emittances and configurations encountered in individual stages of cooling sequences. It is in general possible to demonstrate cooling similar to that expected from the rms equations throughout these cases. However, each of these steps corresponds to cooling by about a factor of  $\sim$ two in 6-D phase space. The total 6-D phase-space cooling that is required is a factor of  $\sim 10^6$ , so, roughly, a total of  $\sim (\ln(10^6) / \ln(2)) = 20$  such steps are required. A three-step configuration with cooling by a factor of  $\sim 15$  is included in this paper, as an initial multistep case.

The eventual goal is to develop complete scenarios which achieve the full cooling requirements. In a complete scenario, the cooling steps are combined with reacceleration and matching sections to form sequences which can obtain cooling by large factors. It is important that these sections do not dilute phase space unacceptably or cause particle loss; it is also important that beam decay loss be limited. R. Palmer has proposed some such scenarios based on the rms cooling equations, but these have not yet been simulated in detail.[8] Substantially different scenarios have also been considered, and still other variations are being developed in the  $\mu$ -cooling discussions.

We plan to adapt and extend the present simulation tools to assist in verifying and developing more complete multistep scenarios. Optimal design will require multiple iterations in configurations; a fast and versatile simulation which can track particle trajectories through multiple configurations and reoptimize is needed and is being developed in the present research program.

## References

1. D. Neuffer and R. Palmer, Proc. 1994 European Particle Accelerator Conference
2. D. Cline, ed. "Physics Potential and Development of  $\mu^+$ - $\mu^-$  Colliders" Sausalito, CA (1994), AIP Conf. Proc. 352 (1995).
3. J. Gallardo, ed. "Beam Dynamics and Technology Issues for  $\mu^+$ - $\mu^-$  Colliders", Montauk, NY 1995, AIP Conf. Proc. 372 (1996).
4. The  $\mu^+$ - $\mu^-$  Collider Collaboration, " $\mu^+$ - $\mu^-$  Collider: A Feasibility Study", BNL-52503, presented at Snowmass Workshop (June 27-July 12, 1996).

5. A. N. Skrinsky and V.V. Parkhomchuk, *Sov. J. Nucl. Physics* 12, 3 (1981), E. A. Perevedentsev and A. N. Skrinsky, *Proc. 12th Int. Conf. on High Energy Accel.*, 485 (1983).
6. D. Neuffer, *Particle Accelerators* 14, 75 (1983), D. Neuffer, *Proc. 12th Int. Conf. on High Energy Accelerators*, 481 (1983), D. Neuffer, *Nucl. Inst. and Meth. A350*, 27 (1994).
7. A. Van Ginneken, *Nucl. Inst. and Meth. A362*, 213 (1995).
8. R. Palmer, unpublished (1995).
9. R. K. Cooper, *Particle Accelerators* 7, 41 (1975).
10. B. F. Bayanov et al., *Nucl. Inst. and Meth.* 190, 9 (1981).
11. D. Neuffer, "Phase Space Exchange in Thick Wedge Absorbers for Ionization Cooling", *Fermilab Pub-96-140* (1996).
12. Particle Data Group: R. M. Barnett et al., *Phys. Rev. D***54**, 1 (1996).
13. R. M. Sternheimer et al., *Atomic Data & Nuclear Data Tables***30**, 261 (1984).

**Figure 1:** Conceptual view of ionization cooling. The beam passes through an absorber where it loses momentum opposite to its motion, decreasing transverse and longitudinal momentum. This is followed by an accelerator section in which only longitudinal momentum is returned to the beam, resulting in a decrease in transverse emittance. Multiple stages of energy loss and longitudinal acceleration can result in beam cooling by large factors.

**Figure 2:** Overview of the beam transformation in passing through a wedge absorber. The upper portion shows a stylized view of a beam passing through a dispersive transport into a wedge absorber; the lower portion shows the projection of the 6-D beam phase space ellipse into  $x$ - $\delta$  phase space, and its changes passing through the system. Dispersion imposes an  $x$ - $\delta$  correlation (ellipse tilt), and the wedge reduces the beam energy  $\delta(x)$ , with energy loss a function of  $x$ :  $\Delta\delta = x dp/ds \tan\theta/p$ . Note that the  $x$ - $\delta$  ellipse area remains the same (in the limit where average energy loss is zero).

**Figure 3.** The sum of the cooling partition numbers  $\Sigma_g = (g_x + g_y + g_L)$  as a function of momentum  $p$  (0—500 MeV/c).  $g_x$  and  $g_y$  are naturally 1 while  $g_L$  becomes strongly negative for  $p < 200$  MeV/c.  $\Sigma_g$  remains greater than 0, which means that ionization loss remains intrinsically cooling at low momenta.

**Figure 4.** Transverse phase space ( $x$ - $p_x$ ) at entrance and exit to the absorber for the case of a 211 MeV/c beam passing through a 20 cm Be absorber with a  $\beta^* = 10$  cm focus at the center. The tilts in the distribution indicates the beam is focusing going into the absorber (and defocusing at the exit). The ( $x$ - $p_x$ ) phase-space density do increases by ~30%, indicating cooling has occurred.

**Figure 5.** Development of energy spread from before to after passing through an absorber for the second case of table 3 (400MeV/c beam going into a 20 cm Be absorber with small initial  $\delta p$  (2 MeV/c)). The increase in energy spread due to energy-straggling is visible, with a “Landau-tail” - a skewed non-gaussian distribution with an extended low-energy tail for particles with large energy losses.

**Figure 6.**  $x$ - $p_x$  phase space distributions at the beginning and at the end of the absorber in the first of case of Table 4 (400 MeV/c  $\mu$  beam going into a 60 cm Be lens absorber). This visually displays the phase-space cooling by a factor of ~1.67. Each of the 4 cases of Table 3 shows similar compression.

**Figure 7.**  $x$ - $E$  phase space before and after a Be wedge at non-zero dispersion (Table 5, case 1). The reduction in energy spread and reduction of dispersion ( $x$ - $E$  slope) are visually displayed.

**Figure 8.** Transformation of phase space ellipses where the wedge is designed to increase energy spread; the wedge is oriented so that lower energy particles go through the thicker end of the wedge.

**Figure 9.** Particle trajectories ( $x$ - $z$  projection) through a solenoid for the sample case of Table 6. The graph shows the  $x$ -component of Larmor orbits (actually helical trajectories). We include 20 cm long transition regions where the longitudinal field rises sinusoidally from 0 to 7 T and the beam develops angular momentum, in addition to the central 60cm long 7 T solenoid. The beam is somewhat mismatched with a focus near the beginning and the end of the solenoid.

**Figure 10.** Transverse phase space at the beginning (a) and at the ends of a sequence of three Be lens/absorbers (b, c, d), showing cooling of the transverse phase space by a factor of 5. (The example of Table 6.) In each absorber the mean beam momentum is reduced from  $\sim 400$  to 200 MeV/c, followed by longitudinal reacceleration after the absorber.

**Figure 11.** Momentum distributions at the beginning (a) and at the ends of the sequence of three Be lens/absorbers (b, c, d) (see Table 6 and Figure 10), showing development of energy straggling over the sequence of energy loss and reacceleration. The momentum spread ( $\Delta p \sim \Delta E/\beta$ ) increases by almost a factor of two and a “Landau-tail” toward lower momenta is observable. However, very few particles are scattered to very small momenta and the increased momentum spread can be cooled with wedges.

Note: In the electronic version of this paper some of these figures are printed upside-down. This is due to incompatibilities between postscript sources and the author’s inexperience in manipulating them. The correct orientation can be deduced from printed text within the figures.

# Ionization Cooling

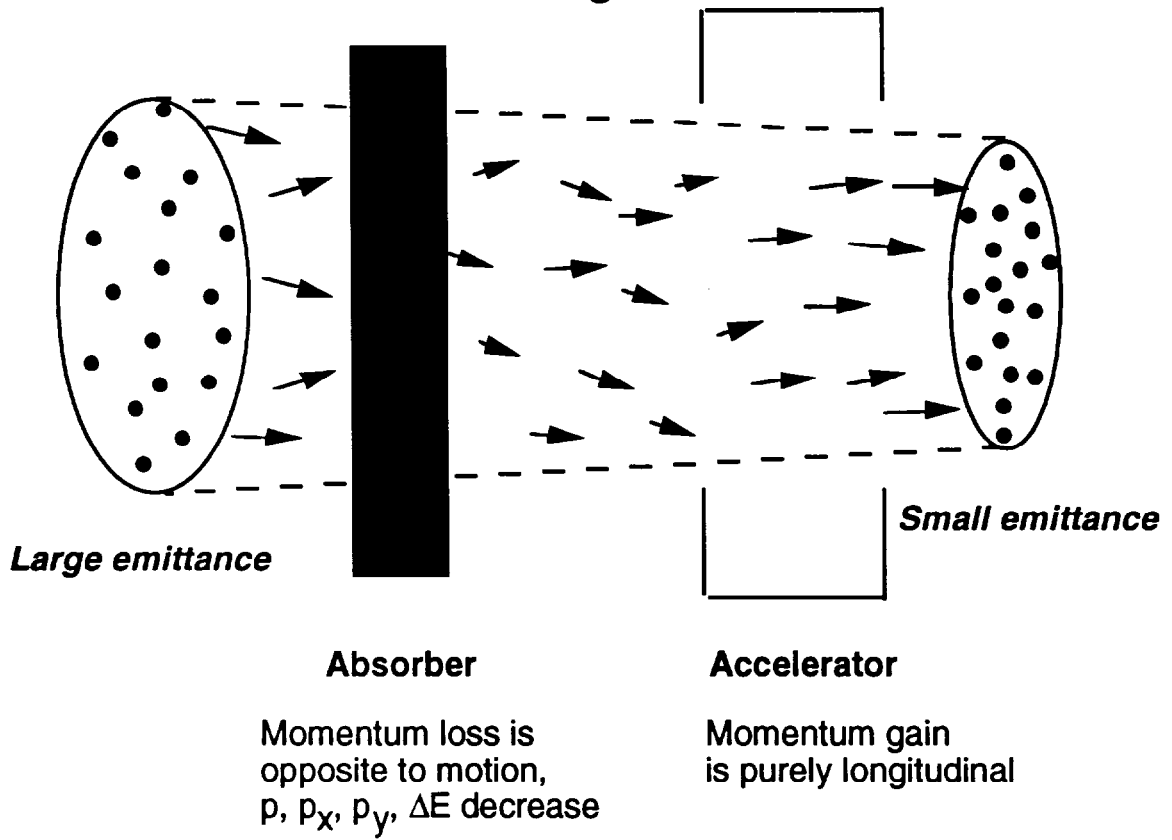


Figure 1

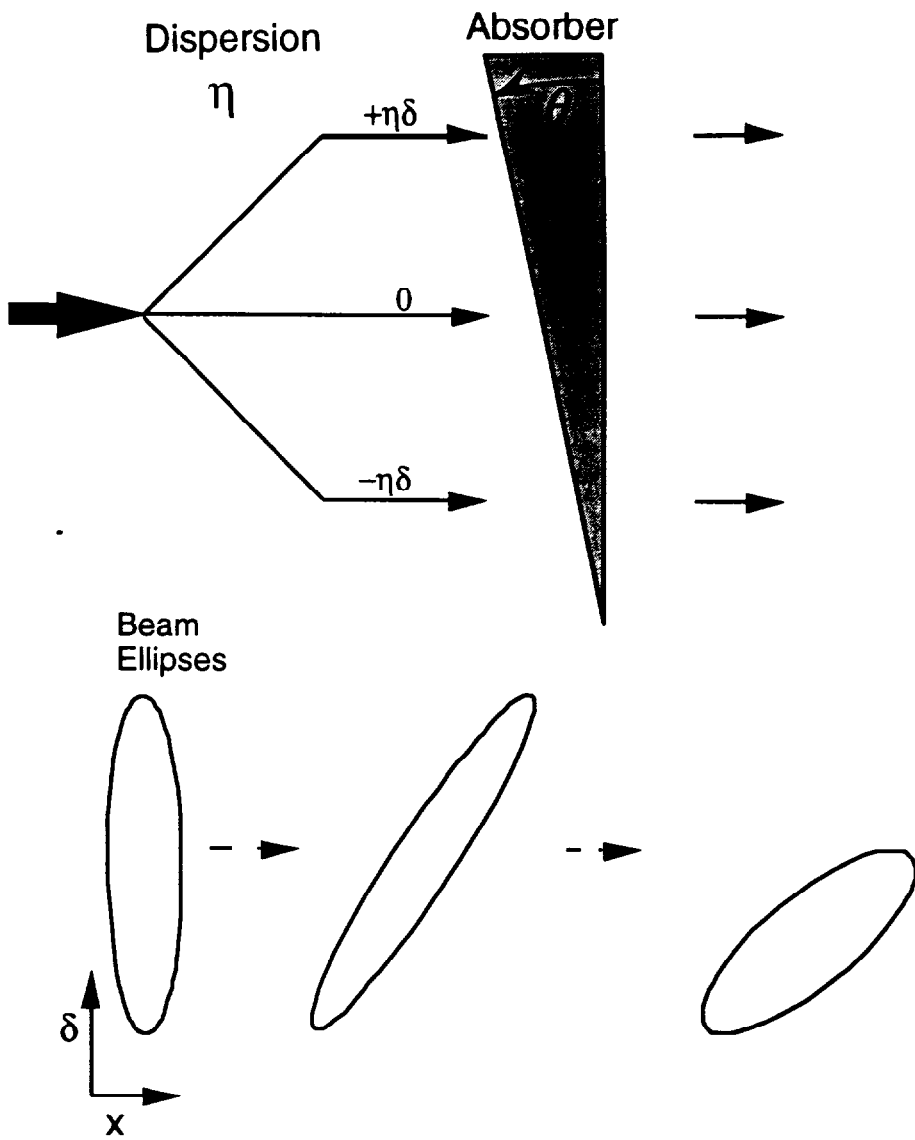


Figure 2

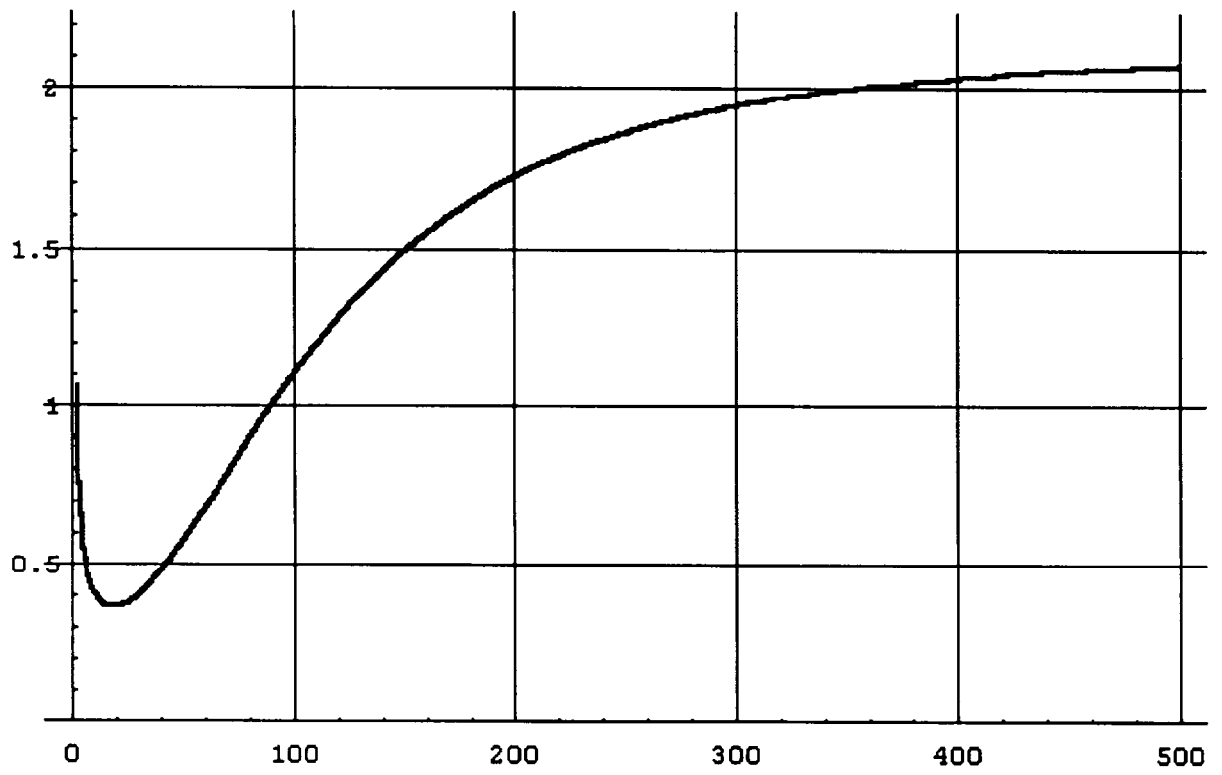


Figure 3

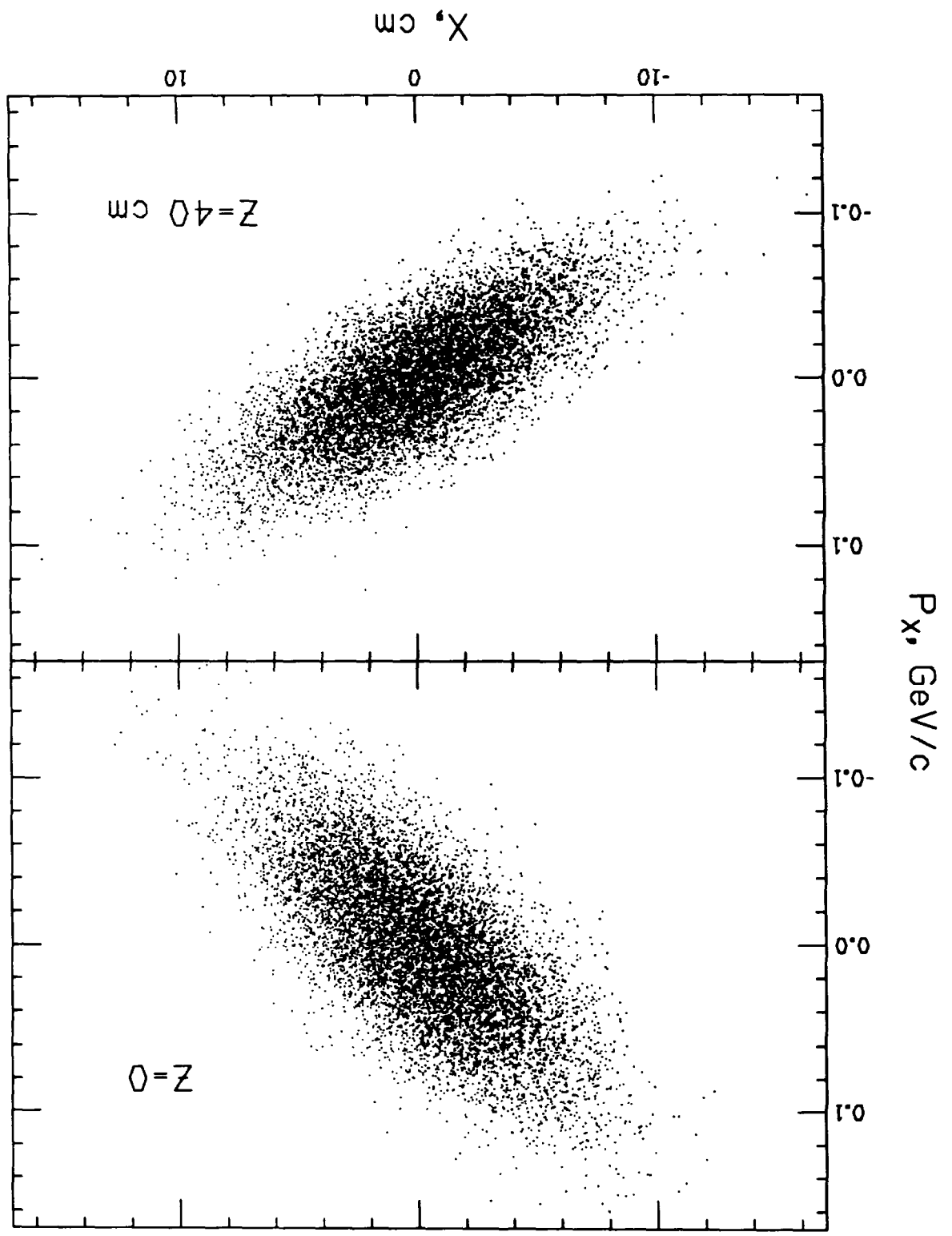


Figure 4

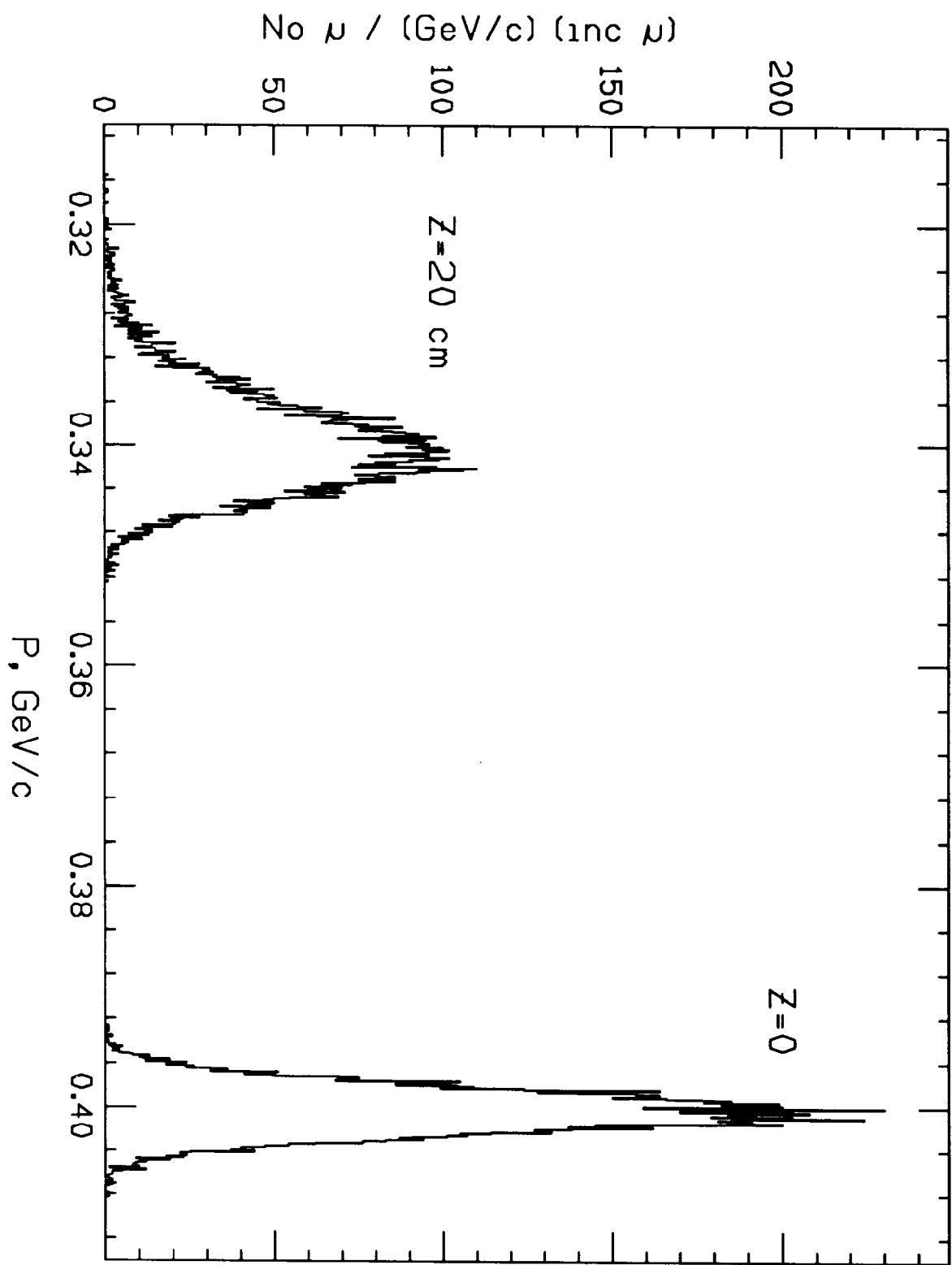


Figure 5

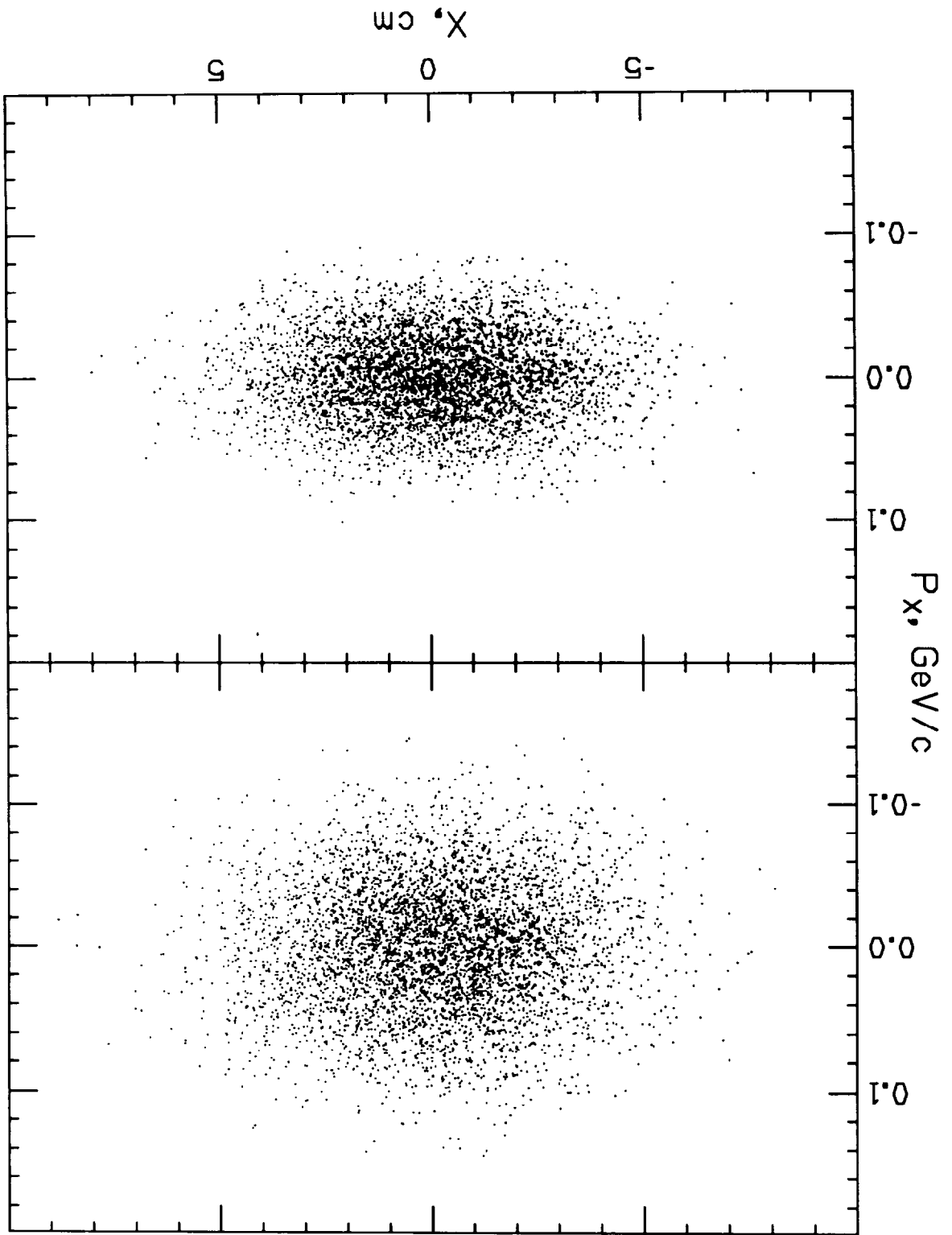


Figure 6

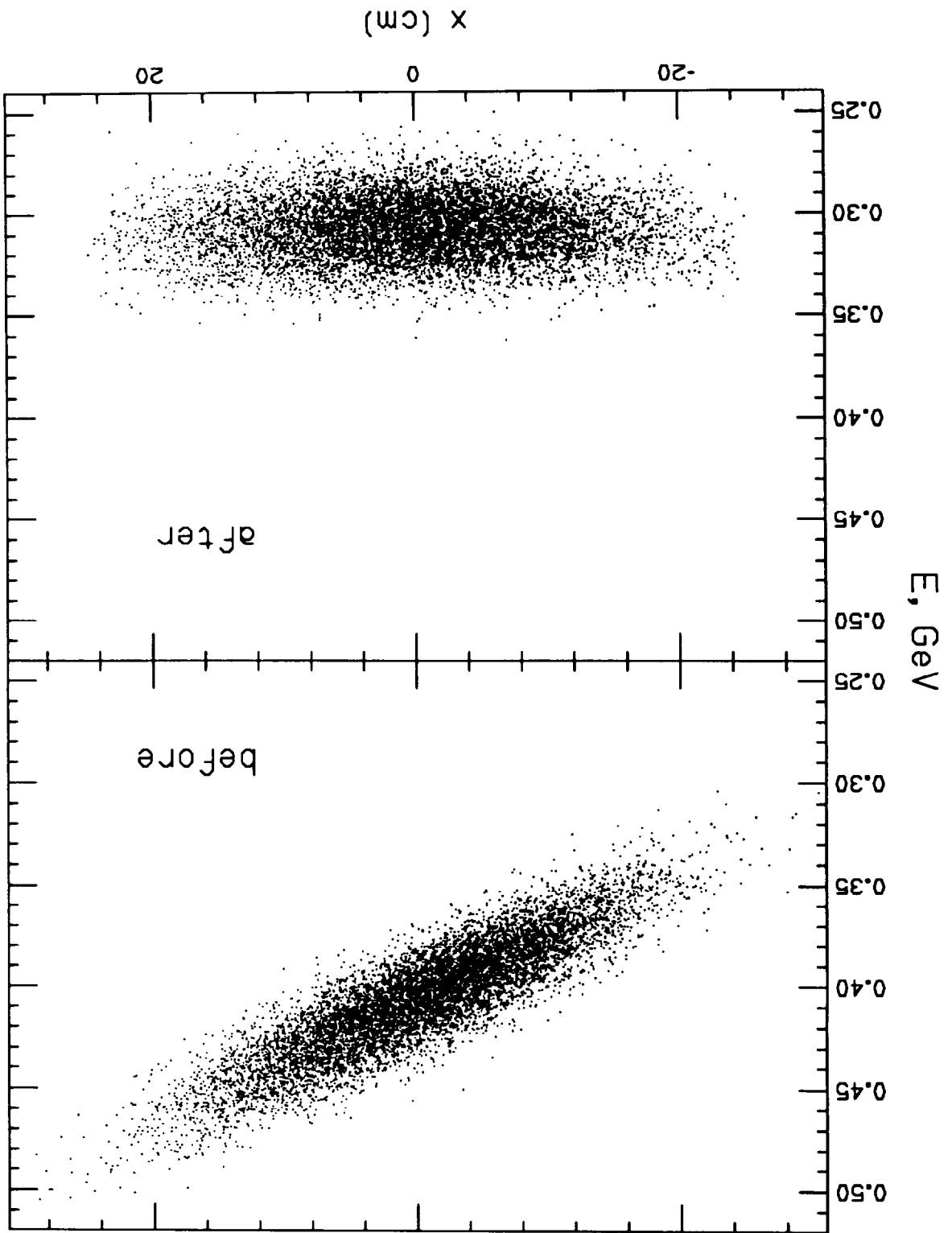


Figure 7

### Beam ellipses in energy-spread increase mode (anti-wedge)

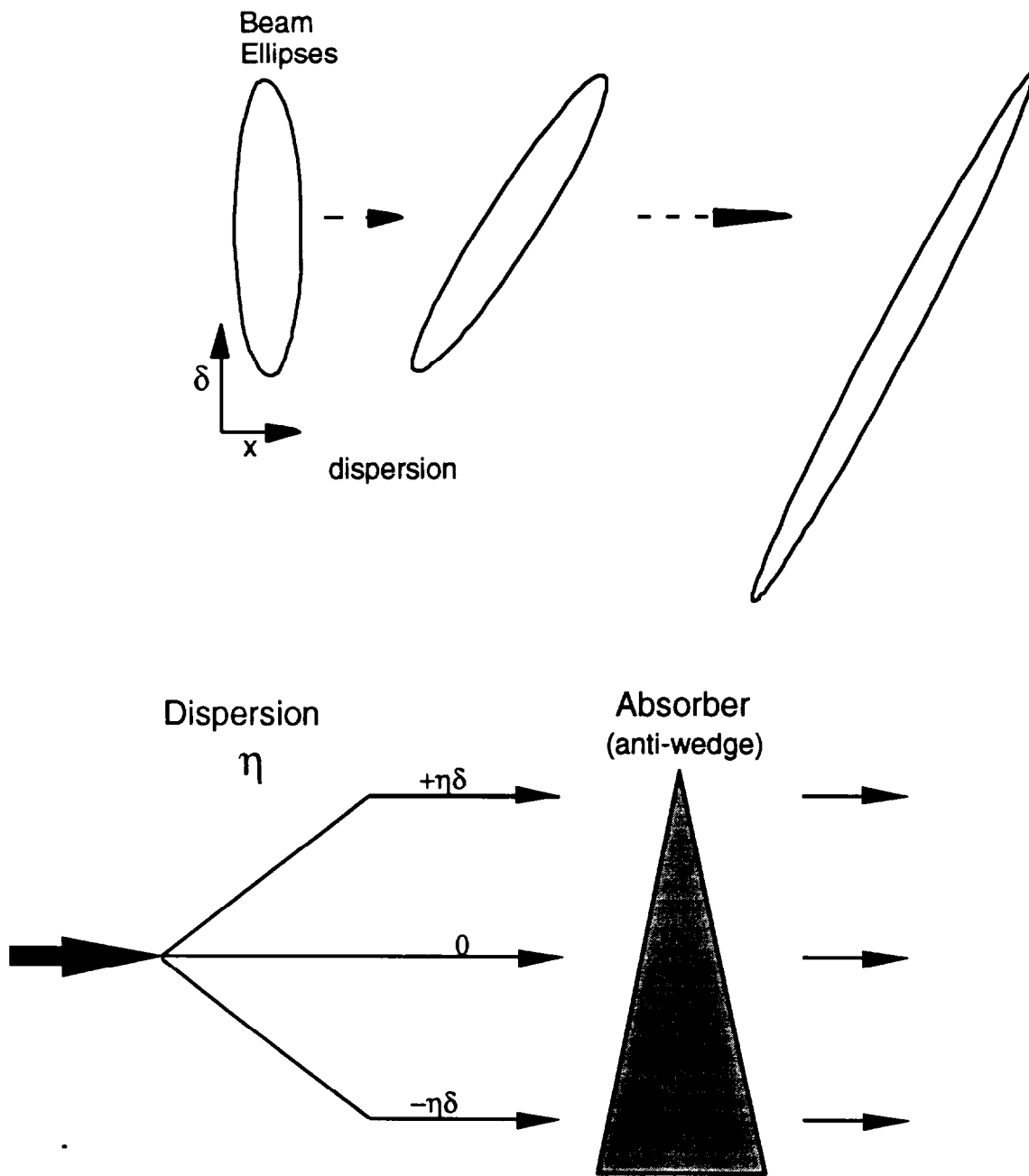


Figure 8

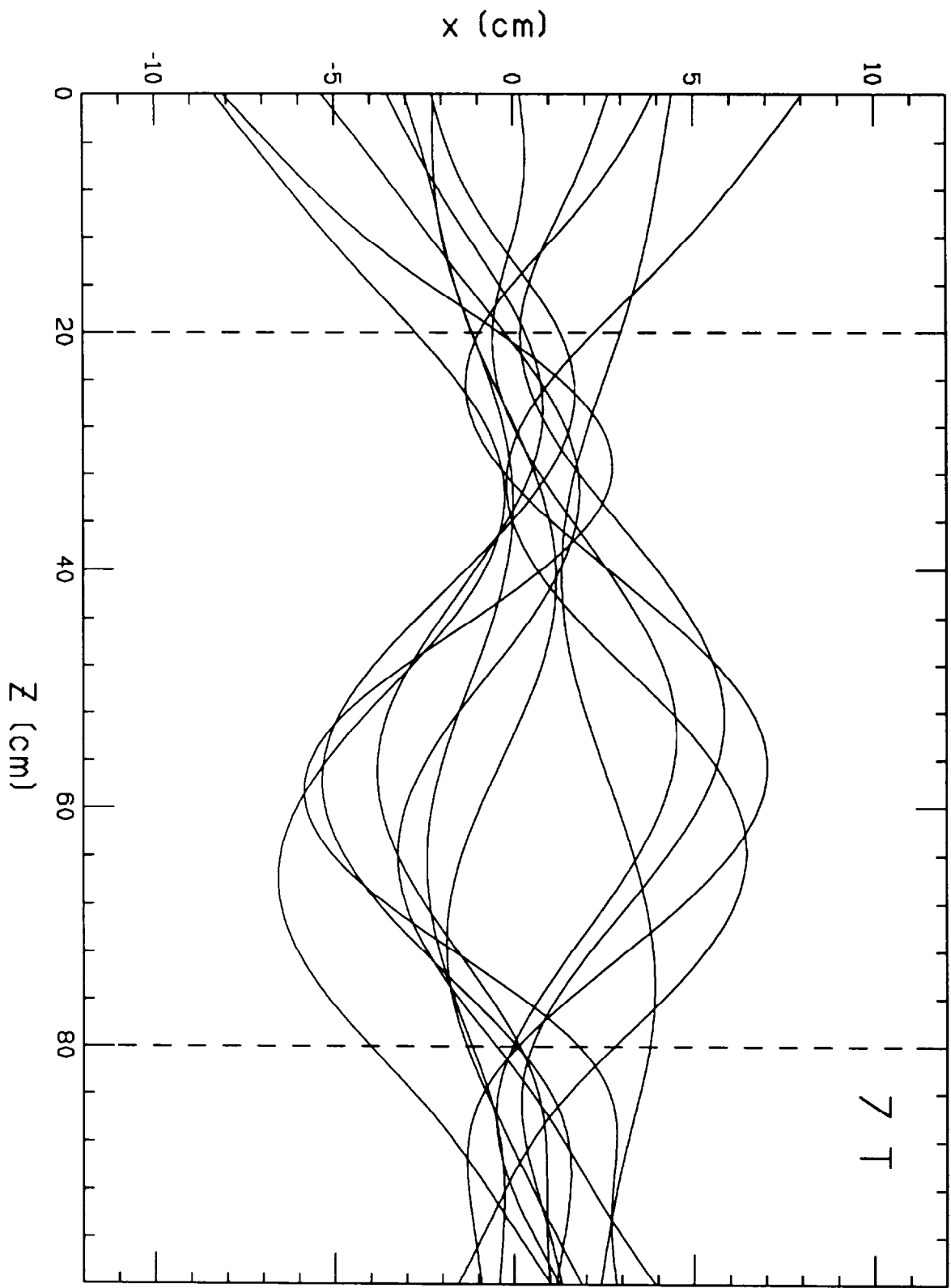


Figure 9

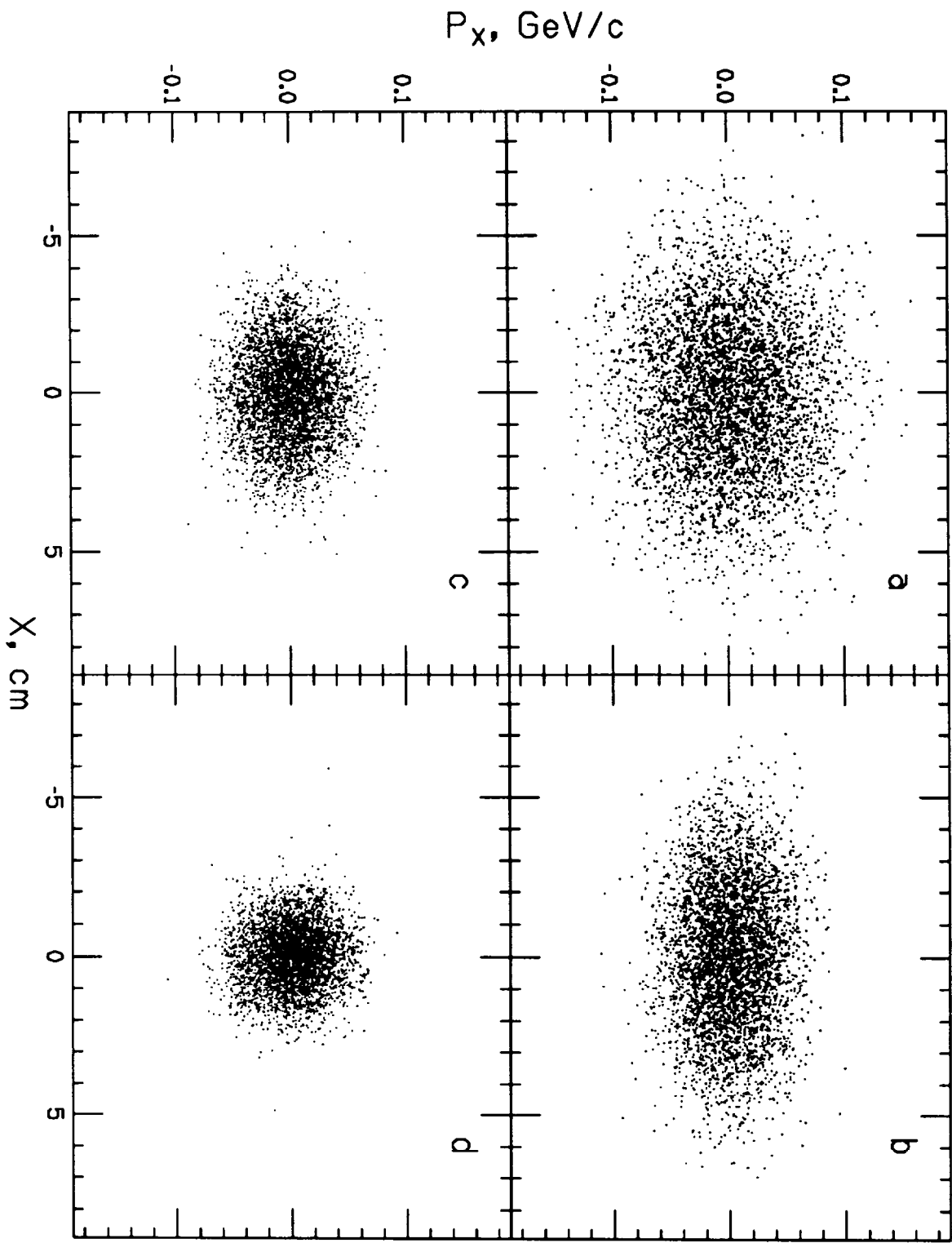


Figure 10

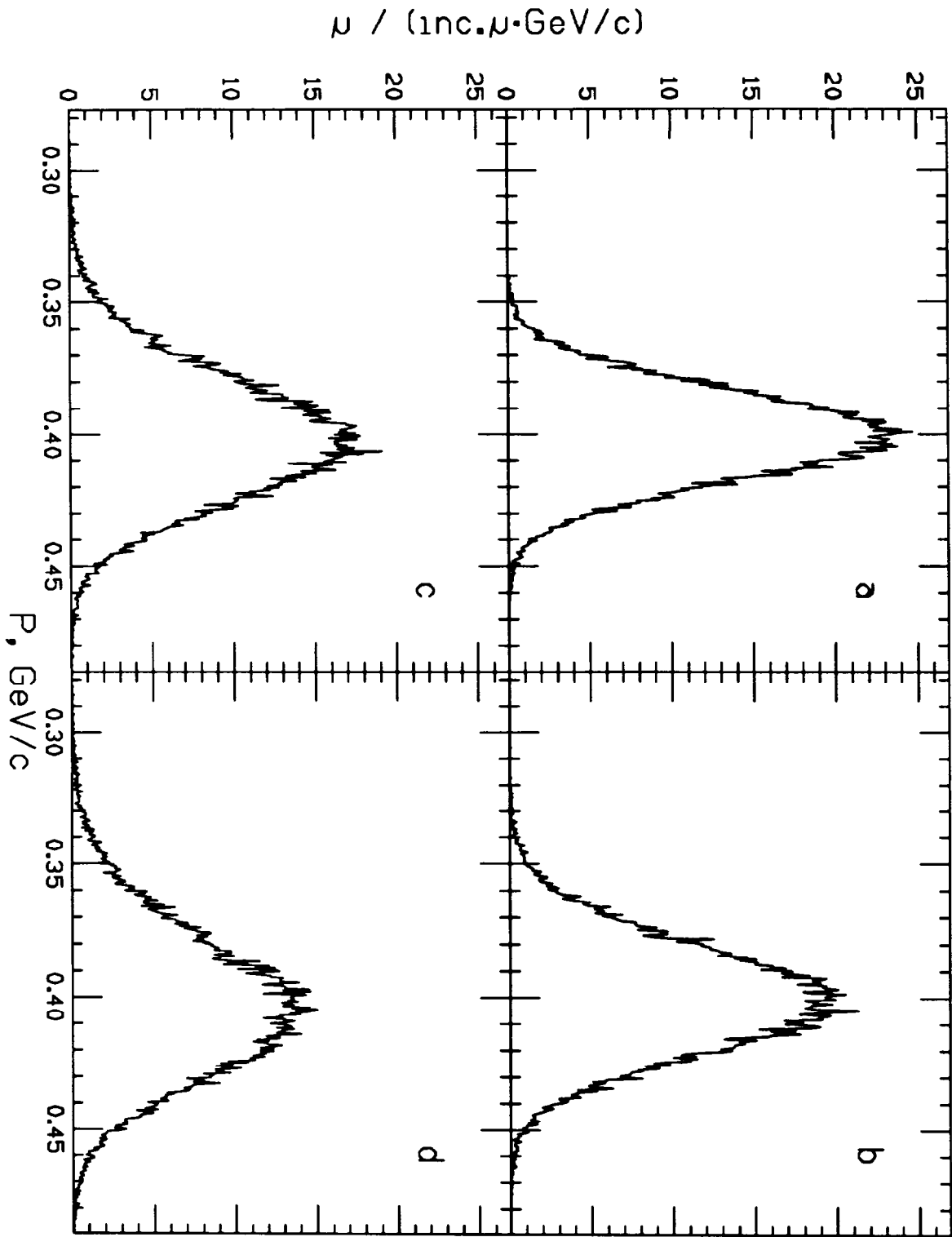


Figure 11